Proceedings of ASME Turbo Expo 2023
Turbomachinery Technical Conference and Exposition
GT2023
June 26-30, 2023, Boston, MA, USA

GT2023-104049

CONSIDERATIONS FOR COMPRESSIBLE FILM COOLING: A COMPUTATIONAL STUDY OF THE EFFECTS OF TRANSONIC FLOWS AND VARYING MAINSTREAM MACH NUMBER

Dale W. Fox[1,*], Michael Furgeson[1], and David G. Bogard[1]

[1]The University of Texas at Austin
Walker Department of Mechanical Engineering
Austin, TX, USA

ABSTRACT

Recent evidence suggests that film cooling flows with engine realistic mainstream Mach number have declined performance in comparison to those with conventional low-speed laboratory conditions. Consideration and understanding of these effects are fundamental to improving film cooling research. The proposed computational study investigates the film cooling performance of a 7-7-7 shaped film cooling hole with respect to varying mainstream Mach number, with constant Reynolds number. The cases studied include mainstream Mach numbers from 0.15-0.75, with a fixed, engine realistic, hole Reynolds number of $Re_d = 10,100$*. Significant results are then evaluated against varying stagnation temperature ratio and blowing ratio. The results showed that at a blowing ratio of 1.75, the adiabatic effectiveness declines significantly with high mainstream Mach number. The decreased performance is due to supersonic flows and shocks in the film cooling hole that disrupt flow in the diffuser section of the hole. These characteristics are observed across all stagnation temperature ratios considered. In addition to these insights, the study discusses the importance of proper thermal scaling and definition of adiabatic effectiveness when operating at high mainstream Mach number. It is demonstrated that the effects of high-speed flow challenge the efficacy of the conventional parameters used to characterize film cooling performance.*

Keywords: film cooling, shaped holes, transonic, compressible, Mach number, heat transfer, fluid mechanics, numerical, RANS, gas turbine engines

NOMENCLATURE

Roman Alphabet

C	Concentration
CFD	Computational Fluid Dynamics
P	Pressure
$RANS$	Reynolds-Averaged Navier-Stokes
T	Temperature
U	Velocity Magnitude
r	Recovery Factor

Greek Alphabet

η	Adiabatic Effectiveness
γ	Specific Heat Capacity Ratio
ρ	Density
χ	Mixture Fraction

Dimensionless Groups

$\mathcal{D}$	Density Ratio
$\mathcal{I}$	Momentum Flux Ratio
$\mathcal{M}$	Blowing Ratio
Ma	Mach Number
$\mathcal{P}$	Pressure Ratio
Re	Reynolds Number
$\mathcal{T}$	Temperature Ratio
$\mathcal{V}$	Velocity Ratio

Superscripts and Subscripts

∞	Mainstream Property
aw	Adiabatic Wall
c	Coolant Property
d	Hole
r	Recovery
$\circ$	Stagnation Condition
s	Static Condition

INTRODUCTION

The gas turbine industry has continuously raised the operational limits within their power turbines over the years, as new manufacturing, materials, and analysis empower engineers to push further. Modern gas turbines operate with gas velocities inside the turbine near the speed of sound, and gas temperatures well in excess of the thermal limits of the metal components. To enable these conditions, turbines have long been actively cooled,

*Corresponding author: dale.fox@solarturbines.com

using bleed air from the compressor to reduce the temperatures of the turbine components, extending their lifetime.

Film cooling is a technique for cooling components by exhausting this bleed gas out through holes in the surface, in the hope that the cooler gas forms a protective film of cold air over the surface. Cooling holes are shaped in order to diffuse the gas across the surface evenly, and to decelerate it to ensure the layer of cool gas mixes out slowly. Understanding the mechanisms of this mixing is key to the understanding of film cooling as a whole. The hole shape has a large impact on the distribution and mixture of coolant, it should be expected that the flowrate, thermodynamic properties, and interactions between the coolant and hot gas layers also has a large impact on the cooling effectiveness.

Studies on Compressible Film Cooling

While many of the other effects on film cooling have been extensively studied, there is a very small set of studies that investigate shaped film cooling holes under compressible conditions. Before the turn of the century, studies that investigated high Mach number film cooling did so with only cylindrical film cooling holes. Liess [1] is a commonly cited study which investigated film cooling up to Mach 0.9, showing very little variation between the different Mach numbers tested. Bauldauf and Scheurlen [2] replicated and extended the results of Liess in a RANS CFD study, confirming that there was little variation in the cases tested.

In the context of shaped film cooling holes, most of the flat plate, compressible film cooling data was performed by the Karlsruhe Institute of Technology. Wittig *et al.*[3], Gritsch *et al.*[4, 5], and Ligrani *et al.*[6], all performed various experiments at Ma_∞ up to 1.2. From these studies, they found that a higher Mach number flow had higher adiabatic effectiveness when other parameters like blowing ratio were matched. They also observed the generation of weak and strong shock wave patterns through shadow-graphs, even with a weakly supersonic mainstream flow. More recently, further experiments were performed at mainstream Mach numbers up to 0.45. Saumweber and Schulz [7] showed that there is a strong impact of Mach number for shaped film cooling holes. The performance decreased substantially for the highest blowing ratio case when the Mach number increased to 0.45, but the behavior was reversed for low blowing ratio, with a smaller but consistent increase in performance.

Separately, Zhou *et al.* [8] investigated multiple density ratios and blowing ratios, and mainstream Mach numbers up to 0.7. They also present the definition of effectiveness with coolant total temperature, relying on pressure sensitive paint (PSP) to make film cooling adiabatic effectiveness measurements. The film cooling holes in this study were cylindrical, rather than shaped. They noted marginal increases in adiabatic effectiveness when going from very low to very high Mach number. Density ratio made a much bigger difference to the behavior of the adiabatic effectiveness, increasing the effectiveness with increasing density.

A final flat plate study of particular note is the computational study by Oliver *et al.* [9]. This was a Large-Eddy Simulation, a model with higher fidelity of capturing turbulence than Reynolds-Averaging provides. This simulation showed a major decrease in the adiabatic effectiveness when raised to a $Ma_\infty = 0.5$, from the baseline case of $Ma_\infty = 0.25$. This was demonstrated to be due to a tendency for the cooling jet to bias to a single side of the hole, poorly distributing the coolant as it exited. The centerline contours clearly show how the film cooling hole reaches supersonic speeds in the high Mach number case, with the indication of shockwaves inside the diffuser.

Present Study

The present study builds on the results of prior compressible flow simulations and experiments, investigating the flow physics within the film cooling hole as the Mach number is raised from incompressible subsonic ($Ma_\infty = 0.25$) to nearly transonic ($Ma_\infty = 0.75$) mainstream speeds. Several cases are performed at $Ma_\infty = 0.75$ with varying blowing ratio $\mathcal{M}$. The blowing ratios chosen are based on those typically observed in low speed shaped film cooling hole studies such as [10–12]. Note that achieving these same blowing ratios at higher Ma_∞ necessitates higher pressure ratio and coolant mass flux, as a result of the increase in mainstream mass flux. As such, the simulation results demonstrate shockwaves are induced within the film cooling hole at even moderate mainstream speeds, and their impact on the flow field and adiabatic effectiveness is discussed. Additionally, the scaling of adiabatic effectiveness and other common film cooling parameters is discussed in the context of compressible flows.

NUMERICAL METHODS

The RANS simulations geometrically consist of a fluid domain, including regions for the mainstream, film cooling hole, and coolant plenum. This domain can be seen in Figure 1. The mainstream domain extends 10 hole diameters upstream and 20 hole diameters downstream of the exit of the film cooling hole, and in the wall-normal direction 15 diameters. The plenum extends five diameters upstream and downstream of the entrance to the film cooling hole, and is 10 diameters long. The entire domain is 6 hole diameters wide, with imposed symmetry conditions at the boundaries to mimic the periodicity of normal film cooling hole arrangements.

The grid was generated within the Fluent meshing tool. Various sizing parameters were applied to different regions of the flow in order to accurately capture the region near the wall, and within the film cooling hole. A cross section of the baseline mesh is shown in Figure 2.

The largest cells of the mesh were in the free stream and coolant plenum, far from the film cooling hole itself. These were set to a size of 2 [mm]. A medium refinement region above and below the film cooling hole was created, and set to a size of 0.1 [mm]. Within the film cooling hole, the cells were further shrunk, to a size of 0.025 [mm]. In addition, a prism layer was created to capture the refinement for the boundary layers near the mainstream and film cooling hole walls. This near wall refinement increased in size exponentially, starting from a first cell height of 2 [μm] until it reached the size of the surrounding cells.

RANS Fluid Dynamic Modelling

The modelling of turbulent kinetic energy in these simulations was based around the realizable k-ϵ model, originally

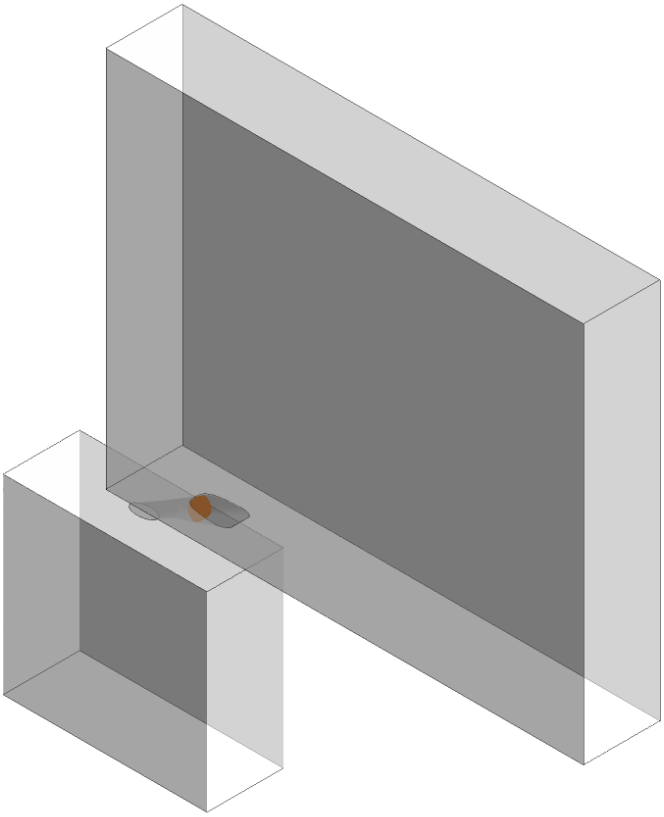

FIGURE 1: PERSPECTIVE VIEW OF FLUID DOMAIN

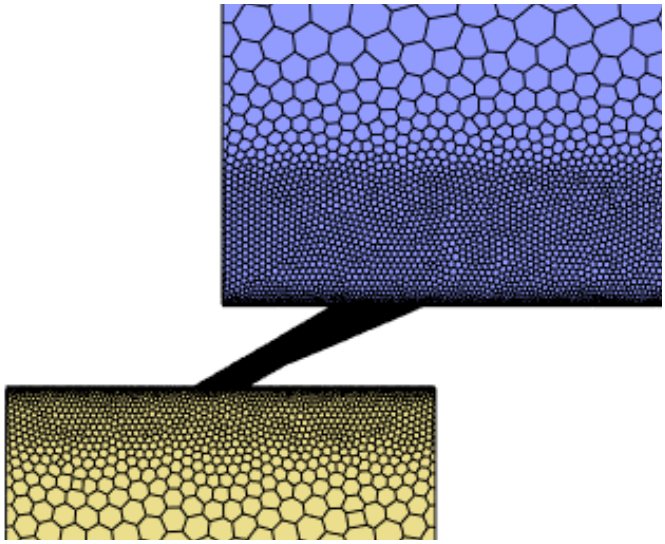

FIGURE 2: MIDPLANE DETAIL OF SIMULATION GRID

developed by Shih *et al.* [13]. This model improves the mixing of turbulent jets over the standard k-ϵ model, modifying the turbulent viscosity model to ensure the kinetic energy remains always positive. Enhanced wall treatment, a scheme developed by Ansys, was used to model the flow near stationary walls [14]. It uses a blending approach, which changes between the usual law of the wall and a linear viscous sub-layer, depending on how thin the first cell is. This enhanced wall treatment works best if the Y^+ of the first cell off the wall is no more than 10. In these simulations, it was verified that Y^+ remains less than 4.1 everywhere in the domain. The peak values, near four, are mostly beneath the coolant jet immediately downstream of the exit of the film cooling hole.

Since the flows in film cooling involve mixing streams with significant temperature differences, it is insufficient to model the fluid properties, like viscosity and thermal conductivity, as constants. Viscosity in these simulations is calculated with Sutherland's law, an empirical correlation for the viscosity of air given a temperature. Since this was a density based simulation, density is one of the fundamental variables in the solution. The constitutive relation between density and pressure used was the ideal gas law. The thermal conductivity was assumed a function of temperature, based on kinetic theory.

The models for discretizing the fluxes between cells have a large impact on the accuracy and simulation time of the RANS simulations. While first order discretization schemes are quick and stable, higher order schemes bring better accuracy. To assist with stability, the simulations were begun with a first order upwinding scheme, running for 250 iterations. Then, the simulation is brought to a second order upwinding scheme and run a further 250 iterations. Finally, the simulation was changed to a so-called MUSCL scheme, which is a blend of a second order upwinding and second order central differencing scheme. The MUSCL scheme helps to suppress oscillations near discontinuities in the flow field (like shock waves). This scheme was used for the final 750 iterations of the simulation.

These simulations are initialized with constant velocities, temperatures, and pressures, split into two separate zones. The mainstream is initialized to zero gauge pressure, the mainstream static temperature, and the mainstream velocity. The film cooling hole and plenum are all initialized to the plenum pressure, coolant temperature, and a small upward velocity. While fluent has a hybrid initialization which is typically used, it was found that hybrid initializing left residual mainstream temperature values in the plenum, which are very slow to rectify due to the slow speed and recirculating regions in the corners of the plenum. It was found that constant value initialization helped reduce these spurious artifacts in the plenum without harming convergence or stability.

Grid Independence and Convergence

In order to determine that the film cooling solution was not dependent on the mesh, a series of three different grids were tested on the same $Ma_\infty = 0.5$, $\mathcal{M} = 1.75$ case. The low and high resolution cases scaled each of the mesh refinements described in the previous section by a fixed value. The relative size between each grid and the next is 1.5. This resulted in a low resolution mesh of approximately 500,000 cells, the baseline mesh of 1,200,000 cells, and a high resolution mesh of 2,800,000 cells.

The error was determined by Richardson extrapolation [15]. This method involves varying the mesh size by a fixed ratio, recording the quantity of interest at every size, and extrapolating

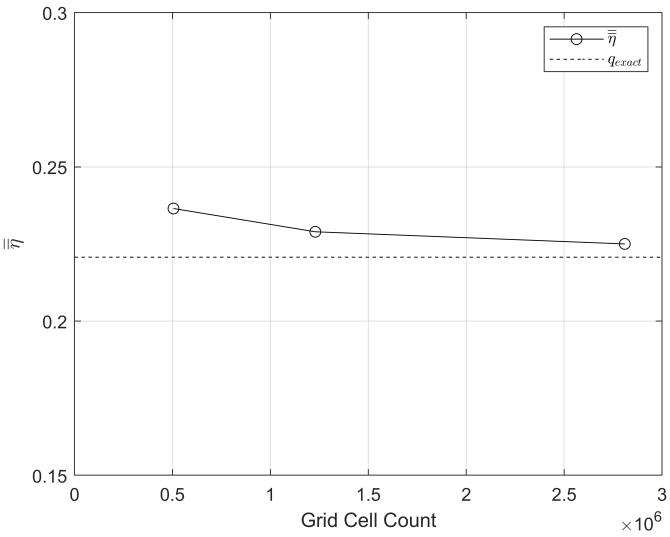

FIGURE 3: VARIATION OF AREA AVERAGED EFFECTIVENESS WITH GRID RESOLUTION

the "exact" value by assuming a error function of the form:

$$q_h - q_{exact} = Ch^p \tag{1}$$

Where C and p are model parameters, q_h is the quantity of interest at mesh resolution h, and q_{exact} is the extrapolated exact value. If the ratio between the mesh resolutions tested is a fixed value r, q_{exact} can be extrapolated by:

$$q_{exact} = \frac{q_0 q_2 - q_1^2}{q_0 + q_2 - 2q_1} \tag{2}$$

For this group of simulations, the quantity of interest used was the average stagnation temperature adiabatic effectiveness of the mainstream wall, $\overline{\overline{\eta^\circ}}$. The details of this definition of effectiveness are discussed later within this paper. The deviation in effectiveness of the baseline grid from the exact solution due to grid resolution was $\delta\overline{\overline{\eta^\circ}} = 0.0082$, which is a percent uncertainty of 3.7% of the baseline $\overline{\overline{\eta^\circ}}$. This error was deemed acceptable, and the baseline mesh was used for the remaining presented cases. The convergence in $\overline{\overline{\eta^\circ}}$ plotted as the grid resolution increased can be seen in Figure 3.

Two convergence criteria were used to assess the number of iterations necessary for a properly converged RANS simulation. Both residuals of the transport equations as well as surface monitors were used to asses the convergence of the simulation.

The residuals for each transport equation were monitored as the solution iterated. For all simulations, the solution was accepted when the residual (iteration-to-iteration change) was on the order of 10^{-5}. All of the simulations reached this, with the residual values generally plateauing between $5 \cdot 10^{-5}$ and $1 \cdot 10^{-5}$. A representative plot of the residuals can be seen in Figure 4a

A surface monitor was also used to verify the stability of the quantities of interest. Namely, the average surface temperature

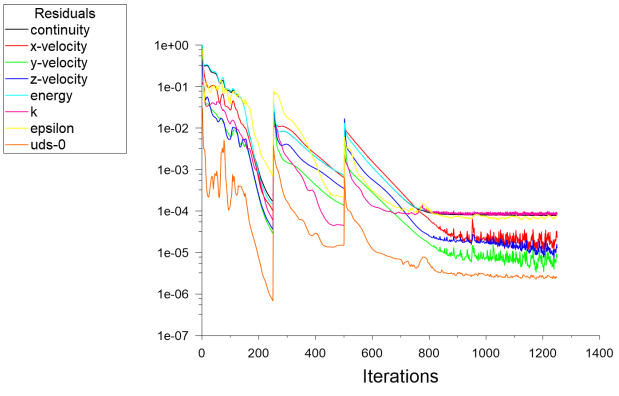

(a) Residual Convergence

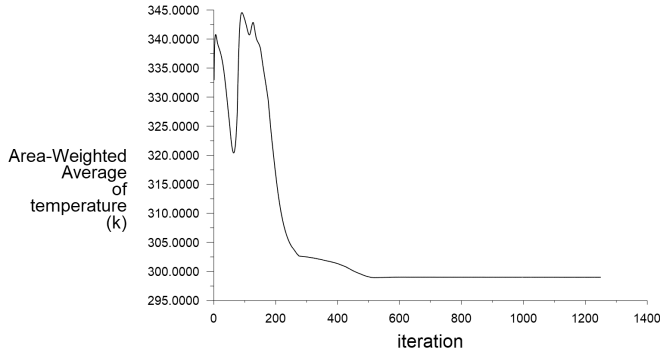

(b) Surface Temperature Monitor

FIGURE 4: REPRESENTATIVE CONVERGENCE CRITERIA

on the film cooled wall was monitored at every time step. The plot of this average quickly stops changing, reaching a consistent value. A plot of the temperature versus the number of iterations can be seen in Figure 4b.

Simulation Conditions

The mainstream inflow condition was a turbulent boundary layer, generated by a secondary simulation run for each Mach number condition. The development distance for this secondary simulation was 40 [mm], intended to match that of the experimental facility. Since the simulations were at fixed hole diameter Reynolds number, the boundary layer thicknesses matched, with a value of approximately 1.05 δ/d, or 1.05 [mm].

The mainstream boundary in both the film cooling simulation and the secondary simulation are zero shear conditions with no outflow. This causes the flow to accelerate slightly from the entrance to the exit of the domains, as the growth of the boundary layer displaces the inviscid flow above. In the film cooling simulation case, the flow is further accelerated by the injection of coolant. The velocity boundary condition at the inlet to the secondary simulation was deliberately reduced to account for this acceleration, with the intent that the average mainstream Mach number on the zero shear boundary would match the targeted value.

The mainstream outflow is a fixed pressure condition, held at a different pressure for each Mach number simulated. These

pressures varied from 57 [kPa] to 327 [kPa], for the highest Mach number case and the lowest Mach number case, respectively. This was done deliberately so that the Reynolds number would remain constant while varying the Mach number. The pressure is modified in inverse proportionality to the velocity, so that the density variation exactly cancels the velocity variation.

Unless otherwise specified, all cases had a mainstream $Re_d = 10,100$. This Re_d was chosen to match the operation of future experimental work. To vary blowing ratio $\mathcal{M}$ and stagnation temperature ratio $\mathcal{T}^o$, a mass flow inlet boundary condition with specified temperature was applied to the entrance of the plenum. Further discussion of the relevance of $\mathcal{M}$ and $\mathcal{T}^o$ appears in later sections.

To assess the validity of the RANS solutions, two baseline cases are compared directly to the LES predictions of Oliver *et al*. [9] in Figure 5. From the figure it may be noted that Mach numbers within the film cooling holes are similar, with large inlet separation regions, peak Mach numbers reached near the entrance to the diffuser, and coolant jetting along the upper interior wall of the hole. At $Ma_\infty = 0.5$, the RANS also demonstrates the oblique shock train that is observable in the corresponding LES case. A notable feature the RANS is missing is the slight detachment of the film cooling jet from the top surface in the higher Mach case. However, this behavior is observed in the RANS simulations as blowing ratio and mainstream Mach number are increased further. With these differences considered, the authors recognize that there are limitations in the accuracy of RANS, notably when modeling high speed flows with known transients [9]. However, the RANS results of this study prove useful in assessing the validity of the following definitions of effectiveness, as well as provide some baseline for expected behavior.

NUMERICAL RESULTS: FILM COOLING ANALYSIS

Several important characteristics of the film cooling problem become more difficult to analyze when observed in a compressible context. The following sections will discuss the behavior of film cooling flow analysis under transonic conditions, using observations from the RANS simulations at varying Mach numbers.

Definitions of Effectiveness

In a normal, incompressible setting for film cooling, the definition of adiabatic effectiveness is straightforward and intuitive:

$$\eta = \frac{T_\infty - T_{aw}}{T_\infty - T_c} \tag{3}$$

This can be viewed simply as a normalization of the difference between the mainstream temperature and adiabatic wall temperature, by the maximum possible difference. This has the property that the value of adiabatic effectiveness is constrained to be between zero and one, where one means that the wall temperature matches that of the coolant, and zero means that it matches the mainstream. In this scenario, the mainstream and coolant temperatures are fixed values that are simple to define and measure, and the overall understanding of the effectiveness is without ambiguity.

However, the transition to compressible flow regimes adds additional energy to the flow field, in the form of the kinetic energy of the fluid. The stagnation temperature is used to account for this additional flow energy at high Mach numbers:

$$T^\circ = T^s \left(1 + \frac{\gamma - 1}{2} Ma^2\right) \tag{4}$$

When considering incompressible flows these two quantities are indistinguishable, as there is no significant kinetic energy to the flow, hence the portion of Equation (4) in parentheses is effectively unity. With this modification, the temperature now represents the sum total of internal and kinetic energy. Another interpretation of this definition is that the stagnation temperature is a fixed upper bound on what the given temperature of a fluid can possibly be. This lends itself to the same idea of normalization that the static temperature was used for in the incompressible scenario.

This then implies that the simplest adjustment to adiabatic effectiveness for compressible flows is to replace the normalizing temperatures with their stagnation quantities:

$$\eta^\circ = \frac{T^\circ_\infty - T_{aw}}{T^\circ_\infty - T^\circ_c} \tag{5}$$

This adjustment should account for the extra kinetic energy of the flow, as mentioned previously. However, viscous dissipation occurs in wall bounded flows of sufficient velocity, diffusing energy within the boundary layer in an irreversible manner, leading to a wall temperature that is not equal to the stagnation temperature. This imperfect temperature recovery can be captured in the recovery factor, r, and used in defining the recovery temperature T^r:

$$T^r = T^s \left(1 + \frac{\gamma - 1}{2} r Ma^2\right) \tag{6}$$

$$T^r = T^\circ \frac{\left(1 + \frac{\gamma-1}{2} r Ma^2\right)}{\left(1 + \frac{\gamma-1}{2} Ma^2\right)} \tag{7}$$

Through empirical measurements and analysis [16], it has been shown that the recovery factor for a standard, flat-plate turbulent boundary layer is the cube root of the Prandtl number, which here is taken to be a constant $r = 0.89$. Modifying the effectiveness to incorporate recovery factor, several issues become obvious that must be addressed to implement a definition that is both usable and clear. To begin to apply the recovery factor to a film cooling problem, equation (7) indicates that three pieces of knowledge are necessary for the recovery temperature, those being the stagnation temperature, the recovery factor, and the Mach number. For lack of a better alternative, the recovery factor is assumed to be that of a boundary layer, and the mainstream stagnation temperatures can be adjusted into recovery temperatures:

$$\eta^{r,\infty} = \frac{T^r_\infty - T_{aw}}{T^r_\infty - T^\circ_c} \tag{8}$$

The question of the coolant is much more complex. The coolant stagnation temperature should be a fixed quantity. It might be argued that the boundary layer recovery factor is sufficient for the coolant, but determining the appropriate reference Mach number

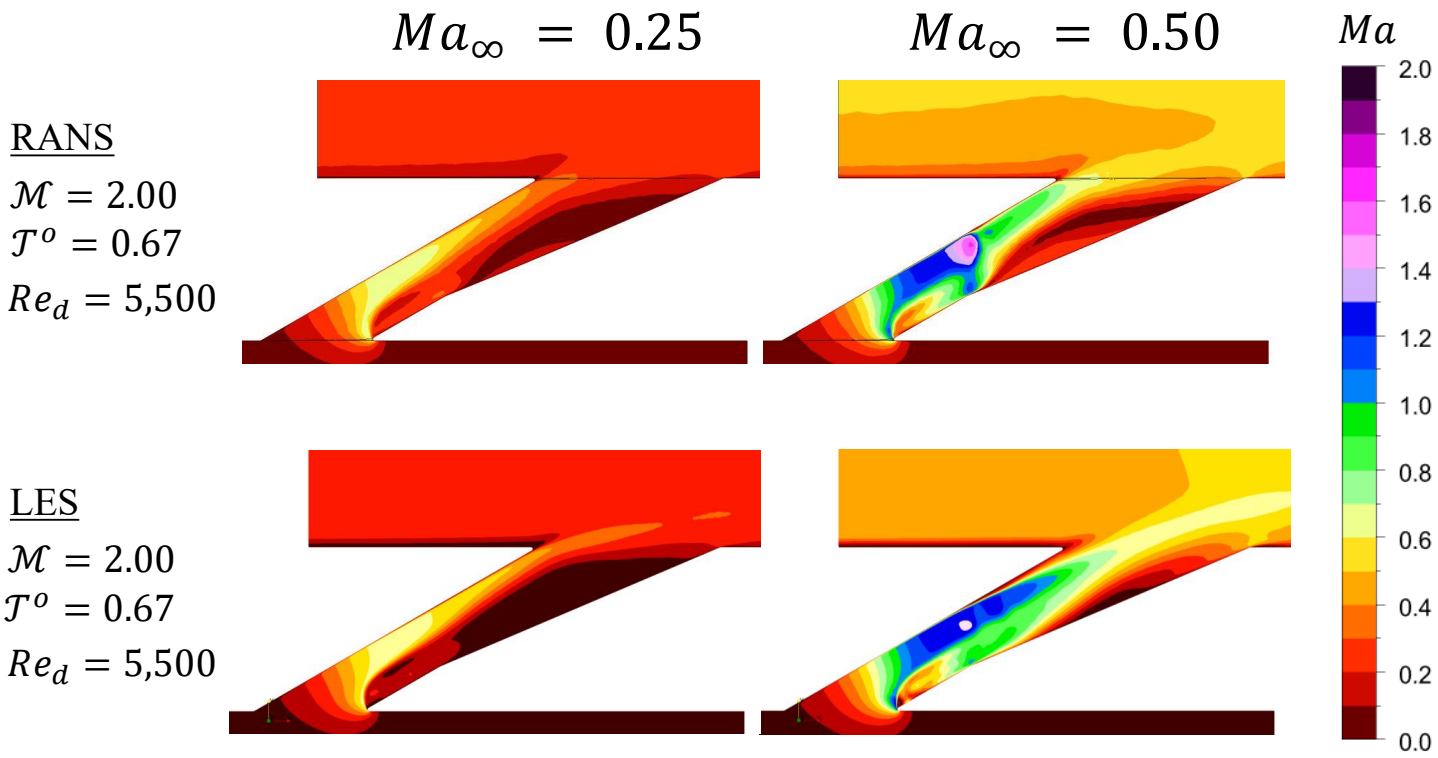

FIGURE 5: COMPARISON OF RANS AND LES [9] MID PLANE MACH NUMBER DISTRIBUTION

of the coolant is difficult. Unlike in the mainstream's case, there is no over-flowing, invisicid stream of coolant that can be treated as a reference value for the computation. Indeed, equation (8) is often the definition that experimental film cooling research arrives at [1, 7, 8, 17–19] for lack of a better option.

While discussing results from experimental facilities, it is important to note the widespread use of mixture fraction as a proxy for the adiabatic effectiveness. The mixture fraction, χ, is a measure of the relative concentration of coolant and mainstream gas:

$$\chi = \frac{C_\infty - C_{aw}}{C_\infty - C_c} \tag{9}$$

The heat/mass transfer analogy implies that the transport equations for heat and species have the same form, and differ only in the rate of diffusion. The diffusivity of heat is related to the Prandtl number, Pr, and the diffusivity of species is related to the Schmidt number, Sc. However, in a turbulent flow field the action of the turbulent eddies acts as a diffusive force in both cases, and generally dominates whatever molecular diffusivity there is. Therefore, it can be reasonable to treat measurements of concentration as though they were measurements of temperature, and the mixture fraction is treated as the adiabatic effectiveness:

$$\eta^\chi = \chi = \frac{C_\infty - C_{aw}}{C_\infty - C_c} \tag{10}$$

However, in compressible flows the analogy is less direct, due again to the viscous dissipation action within the boundary layer. Kinetic energy is dissipated as heat, and causes the recovery temperature phenomenon discussed previously. However, there is no source of "kinetic concentration" or "concentration dissipation" in the equations or reality of mass transport. Since the initial values of concentration can only be mixed, not dissipated away, the mixture fraction can be interpreted as to an effectiveness based entirely on stagnation temperatures:

$$\eta^\chi = \frac{T^\circ_\infty - T^\circ_{aw}}{T^\circ_\infty - T^\circ_c} \tag{11}$$

Where the "wall stagnation temperature" is simply a mixture of the mainstream and coolant stagnation temperatures:

$$T^\circ_{aw} = \chi T^\circ_\infty + (1-\chi)\, T^\circ_c \tag{12}$$

This is subtly different from the stagnation temperature definition of (5), in what the wall value is meant to represent. Whenever there is a statement of effectiveness based upon concentration data - like PSP and other techniques - Equation (11) is being represented.

Returning to temperature-based definitions of effectiveness, an attempt has been made in this analysis to rectify the mainstream recovery temperature definition of effectiveness in equation (8). In attempting to account for recovery effects of the coolant, it was mentioned that a Mach number that represents the coolant is difficult to identify. It would be erroneous to assume that the mainstream and coolant share a reference Mach number. There is no guarantee that a hypothetical inviscid reference point would match either the velocity or the temperature of the mainstream. In general, these quantities are completely independent from those of the mainstream.

However, an attempt to determine the reference Mach number *a priori* can be made with a few assumptions and the isentropic

Mach relations from inviscid compressible theory. The isentropic Mach number relations are analogous to the Bernoulli equation, but for compressible flow. Under the assumption of an ideal, isentropic flow with an ideal gas, the ratio between the gas' total pressure and static pressure can be determined from its Mach number:

$$\frac{P^\circ}{P^s} = \left(1 + \frac{\gamma - 1}{2} Ma^2\right)^{\frac{\gamma}{\gamma-1}} \tag{13}$$

This is the same analysis that the stagnation temperature definition of equation (4) is based upon. Now, in a film cooling scenario, the stagnation-to-static pressure ratio of the coolant is closely linked to the pressure ratio $\mathcal{P}$, which is the ratio between coolant and mainstream pressures. If it is assumed that the coolant expands isentropically from the plenum through the film cooling hole, then these two ratios are equivalent. Then, this pressure ratio is treated as the driving pressure for the isentropic expansion of equation (13), and the formula can be rearranged to calculate an isentropic Mach number, Ma^{isen} from a given pressure ratio:

$$\begin{aligned}
\mathcal{P} = \frac{P^\circ}{P^s} &= \left(1 + \frac{\gamma - 1}{2} Ma_c^2\right)^{\frac{\gamma}{\gamma-1}} \\
\mathcal{P}^{\frac{\gamma-1}{\gamma}} &= 1 + \frac{\gamma - 1}{2} Ma_c^2 \\
\mathcal{P}^{\frac{\gamma-1}{\gamma}} - 1 &= \frac{\gamma - 1}{2} Ma_c^2 \\
\frac{2}{\gamma - 1}\left(\mathcal{P}^{\frac{\gamma-1}{\gamma}} - 1\right) &= Ma_c^2 \\
Ma_c^{isen} &= \sqrt{\frac{2}{\gamma - 1}\left(\mathcal{P}^{\frac{\gamma-1}{\gamma}} - 1\right)}
\end{aligned} \tag{14}$$

Using this Mach number, the assumed recovery factor of $r = \sqrt[3]{Pr}$, and the coolant stagnation temperature, the adiabatic effectiveness can be adjusted to use recovery temperature for each scaling variable:

$$\eta^r = \frac{T_\infty^r - T_{aw}}{T_\infty^r - T_c^r} \tag{15}$$

Where T_c^r is:

$$T_c^r = T_c^\circ \frac{1 + \frac{\gamma-1}{2} r Ma_c^2}{1 + \frac{\gamma-1}{2} Ma_c^2} \tag{16}$$

This is a straightforward analysis, but has not previously been developed within the film cooling literature. There are also a number of inherent issues with the assumption of an isentropic expansion. First, this study has already clearly demonstrated the formation of shock waves within the film cooling holes at the higher Mach conditions, which immediately breaks the isentropic assumption for those cases. There is no way to know beforehand whether there will be a shock or not, so that cannot be included in the coolant temperature analysis. Even if the coolant never shocked, a fixed coolant Mach number is only valid in the case of a flat plate, zero-pressure gradient flow. On actual engine components like blades and vanes, the acceleration and deceleration of the mainstream flow around the blade implies the coolant should also accelerate and decelerate, and it would be necessary to track a profile of the coolant Mach number distribution along the surface.

Using all the definitions of effectiveness above, a comparison of the resulting adiabatic effectiveness contour at $Ma_\infty = 0.75$ is shown in Figure 6. Inspection of the stagnation temperature definition immediately shows the issue in not accounting for recovery temperature, in the non-zero effectiveness outside of the path of the jet. The mainstream recovery temperature definition is more like a "normal" contour of adiabatic effectiveness. The adjustment to coolant recovery temperature reduced the apparent effectiveness at the center of the jet in the highest Mach number cases, mimicking the results of the mixture fraction contour. This similarity occurs despite the mechanism for the reduced effectiveness being different. In the mixture fraction, the apparent effectiveness is reduced because the surface temperature is actually a mixture of the stagnation values, so no viscous dissipation has affected the value. In the recovery temperature definition, the coolant temperature used to normalize the effectiveness has decreased, which has the effect of reducing the apparent value of effectiveness within the jet.

Further comparison can be made across the range of operating conditions by taking a spatial average of the effectiveness, over a downstream distance that starts 5 hole diameters downstream and ends 20 diameters downstream. This is shown in Figure 7. In the low Mach number range, the different definitions cluster more closely together. There is still minor variation, with the mixing fraction definition the lowest of the four. The definitions diverge as mainstream Mach number increases, with the stagnation temperature definition being significantly higher than the other three definitions at $Ma_\infty = 0.75$. The mixing fraction and recovery factor definitions remained the most consistent with each other at high Mach numbers, as supported by Figure 6. The mainstream recovery factor definition has a consistent trend but higher average effectiveness than the definition that uses coolant recovery factor, as should be expected.

Density and Temperature Ratio Scaling

While the blowing ratio, $\mathcal{M}$, is widely used for scaling film cooling and remains well defined in compressible scenarios, the velocity ratio $\mathcal{V}$ and momentum flux ratio $\mathcal{I}$ are also widely used in incompressible film cooling literature, but become difficult to quantify in transonic film cooling. The crux of the issue is knowledge of the density of the coolant involved in these scaling parameters. Incompressible film cooling has constant density from the entrance to the exit of the film cooling hole, and thus can use observations of the temperature and pressure in any location within the coolant supply to define the density of the coolant. In compressible film cooling, the density can be seen widely varying as the coolant accelerates and decelerates. As a comparison, Figure 8 shows how the different Mach numbers, with a fixed blowing ratio and coolant stagnation temperature ratio, vary in exit plane density. The local density ratio relative to the mainstream gas at the exit of the holes at different Mach numbers indicate a widely varying density for the same nominal operating conditions, from approximately 1.2 to nearly 1.4. This variation is the difficulty in defining and using density ratio as a scaling parameter.

Oliver *et al.* [9] adopted an alternative parameter to use when matching between low and high Mach number cases, which is the

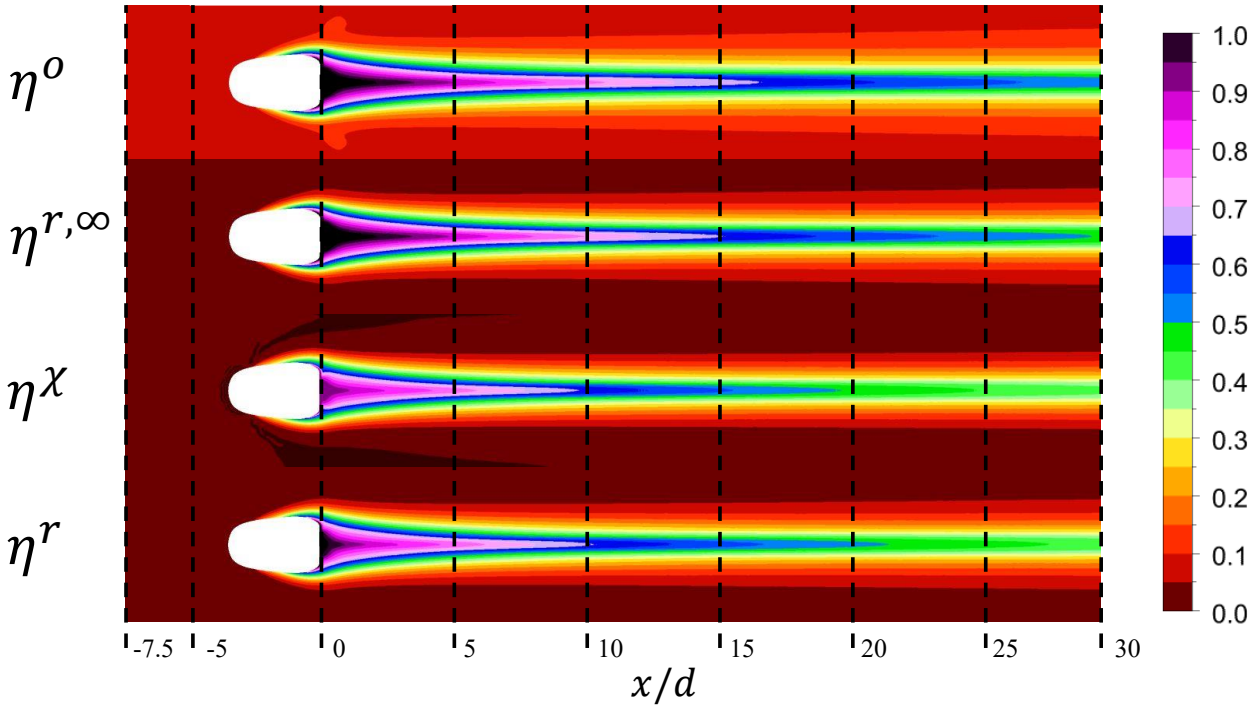

FIGURE 6: CONTOURS OF ADIABATIC EFFECTIVENESS FOR VARYING DEFINITIONS OF η. Ma_∞ = 0.75

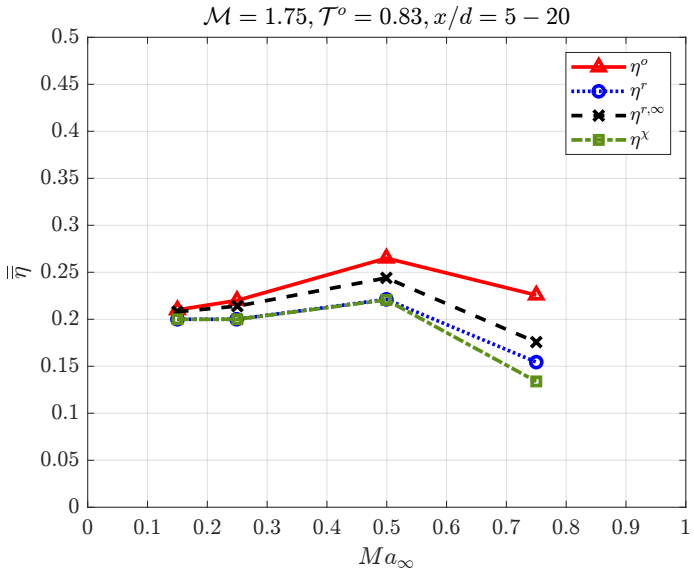

FIGURE 7: AREA AVERAGED EFFECTIVENESS FOR VARYING MACH NUMBER

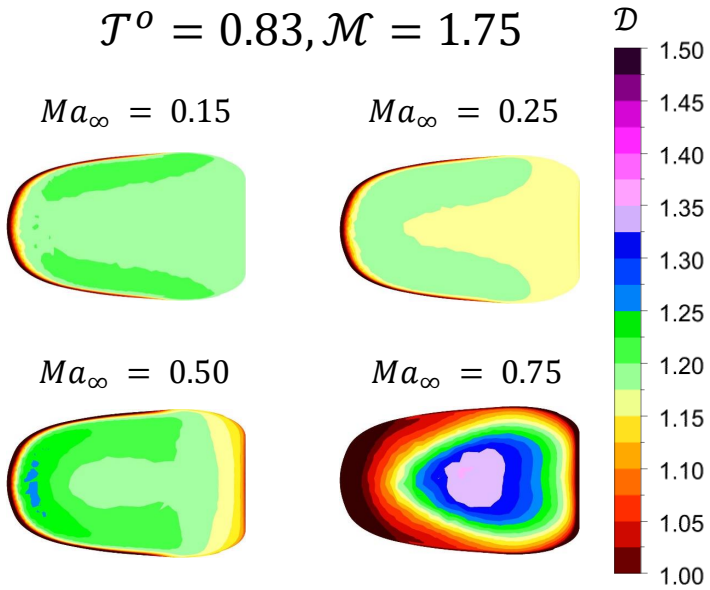

FIGURE 8: EFFECT OF Ma_∞ ON EXIT PLANE DENSITY RATIO

stagnation enthalpy or stagnation temperature ratio.

$$\mathcal{T}^\circ = \frac{T_c^\circ}{T_\infty^\circ} \tag{17}$$

Discussion of this scaling parameter is rare in the literature, but exists in some other studies such as that of Ornano & Povey [20]. The authors of that study evaluate $\mathcal{T}^\circ$ under incompressible flow conditions, but stress the importance of studies which examine the compressible flow regime. As such, for constant specific heat and incompressible flows, the stagnation temperature is the same as the static, and thus the stagnation temperature ratio is equivalent to the density ratio under these conditions. However, when they diverge they have differing meaning. While the density ratio is obviously the relative density of the two gas streams, the temperature ratio is a representation of the relative energy content

convected by the gases. For this study, the stagnation temperature ratio is used to scale cases due to its consistency of definition at high Mach number.

NUMERICAL RESULTS: FLOW FIELD OBSERVATIONS

This section of the results describes the flow behavior observed while varying mainstream Mach number, blowing ratio and stagnation temperature ratio.

Mach Number Contours

Cross sections of Mach number at the midplane are shown in Figure 9. In this figure, the blowing ratio and stagnation temperature ratio are held constant. The contours of Mach number for $Ma_\infty = 0.15$ and $Ma_\infty = 0.25$ in Figure 9 can be taken as typical incompressible shaped film cooling hole flow fields at the mid plane. A film cooling hole with a sharp inlet will nearly always create a separation region, as seen in the low Mach number region near the entrance to the hole. The main body of the film cooling jet rises over this region, accelerating due to the restriction in area imposed by the separation. Once the jet enters the diffuser section, the flow reduces in speed, spreading outward into the larger area of the diffuser. This speed reduction minimizes the shear between the mainstream and the film cooling jet, which should minimize the mixing rate of the coolant as it travels downstream. The forward expansion angle of the diffuser also induces the jet to turn downward slightly, causing the jet to become more parallel with the mainstream flow as it exits the hole. However, as the mainstream Mach number increases, the character of the flow inside the film cooling hole shows distinct differences. In the $Ma_\infty = 0.5$ case in Figure 9, the jet accelerates, as before, but reaches much higher Mach numbers. This may be expected as for constant blowing ratio, an increased mainstream Mach number implies an increased coolant Mach number. However, the $Ma_\infty = 0.5$ case crosses the sonic velocity threshold, rising to a peak Mach number at the entrance to the diffuser of $Ma = 1.5$. It is key to recognize the transition from subsonic to supersonic flows as a key shift in the behavior of the jet with relation to the diffuser. In a subsonic scenario, an area increase like the diffuser causes the film cooling jet to decelerate, as mentioned before. However, a supersonic flow accelerates as area increases. This acceleration is seen immediately as the jet enters the diffuser, and is not observed in the subsonic cases. Further complicating the flowfield inside the diffuser is, immediately after the entrance, there is an abrupt deceleration to subsonic velocities. This is indicative of a normal shock wave. After the shock, the subsonic flow decelerates within the diffuser as in the subsonic cases, and meets the mainstream at a relatively sedate velocity, at least compared to that seen within the film cooling hole itself.

The Mach number field of the $Ma_\infty = 0.75$ case further complicates the supersonic interactions of the jet. Seen in Figure 9, the main body of the jet accelerates to even higher Mach numbers, reaching as high as $Ma = 2$. With the enhanced acceleration, the jet shows indications of an even stronger shock pattern. Immediately after the first shock, a pattern is visible, reminiscent of a shock diamond exiting a rocket nozzle. The strength of the shock in this case has detached the jet from the upper wall, causing it to deflect toward the center of the diffuser, and giving rise to a new separation region above the jet, in addition to the separation below the jet present in every simulation. This separation region is reducing the effectiveness of the diffuser in decelerating the flow, and the net effect is that the jet exits the hole at a shallower angle and higher velocity than the rest of the cases. Furthermore, as the jet remains supersonic at the exit of the hole, a weak expansion fan is predicted at the trailing edge, limited by a separation region on the mainstream surface.

Additional Mach number distributions within the hole are shown in Figure 10, using the highest Mach number tested of $Ma_\infty = 0.75$ and varying the blowing ratio. The development of a shock wave may be observed with increasing blowing ratio, where it is shown that flow is supersonic at blowing ratios as low as $\mathcal{M} = 1.00$. As the blowing ratio increases, the standing shock wave moves further into the diffuser and encompasses a larger area, displacing the separation region beneath the jet at the highest blowing ratio shown in the figure of $\mathcal{M} = 2.00$. Although not shown for brevity, as the blowing ratio is increased to $\mathcal{M} = 2.50$ and $\mathcal{M} = 3.00$, the shock wave begins to encompass the majority of the diffuser.

Contours of the Mach number distribution spanwise across the hole at the entrance and exit of the diffuser section are shown in Figure 11. The progression of coolant Mach number within the hole may be observed as blowing ratio increases. At the lowest blowing ratio case, the flow remains subsonic throughout the diffuser. At $\mathcal{M} = 1.00$, the flow transitions to supersonic speeds entering the diffuser, but decelerates to subsonic speeds by the end of the diffuser. Finally, at $\mathcal{M} = 2.00$, the flow remains supersonic through the entire diffuser, leaving a separated jet core. Although again not shown for brevity, it is noteworthy that for $\mathcal{M} > 1.25$, the Mach contour at the entrance to the diffuser becomes choked, or area limited. This effect is supported by comparison of Figures 9 and 10, where it may be observed that for $\mathcal{M} = 1.75$ and $\mathcal{M} = 2.00$, the Mach contours are approximately the same up until the diffuser. Consequently, the increase in mass flux through the hole at these higher blowing ratios is due to increasing coolant density, made possible by increased coolant supply pressure.

These distinct flow features at high Mach number have large impacts on the downstream effectiveness of the film cooling holes under these conditions, which will be shown in the area averaged plots in the next section.

Adiabatic Effectiveness

The following comparisons of area averaged effectiveness will be presented using the recovery temperature definition of adiabatic effectiveness, η^r. Although all definitions scale similarly with the conditions tested, η^r was best bounded between 0 and 1 among the thermal forms of effectiveness. Figure 12 shows the variation of area averaged η^r for all blowing ratios simulated, at two different stagnation temperature ratios. All cases in this comparison were at the highest Mach number of 0.75. While the trend between cases is similar when scaling with blowing ratio, it can be seen that $\mathcal{P}$ more closely aligns the effectiveness from different temperature ratios.

Further, a large decrease in the effectiveness is seen at $\mathcal{P} = 2.50$, which is due to the jet seperation induced by the

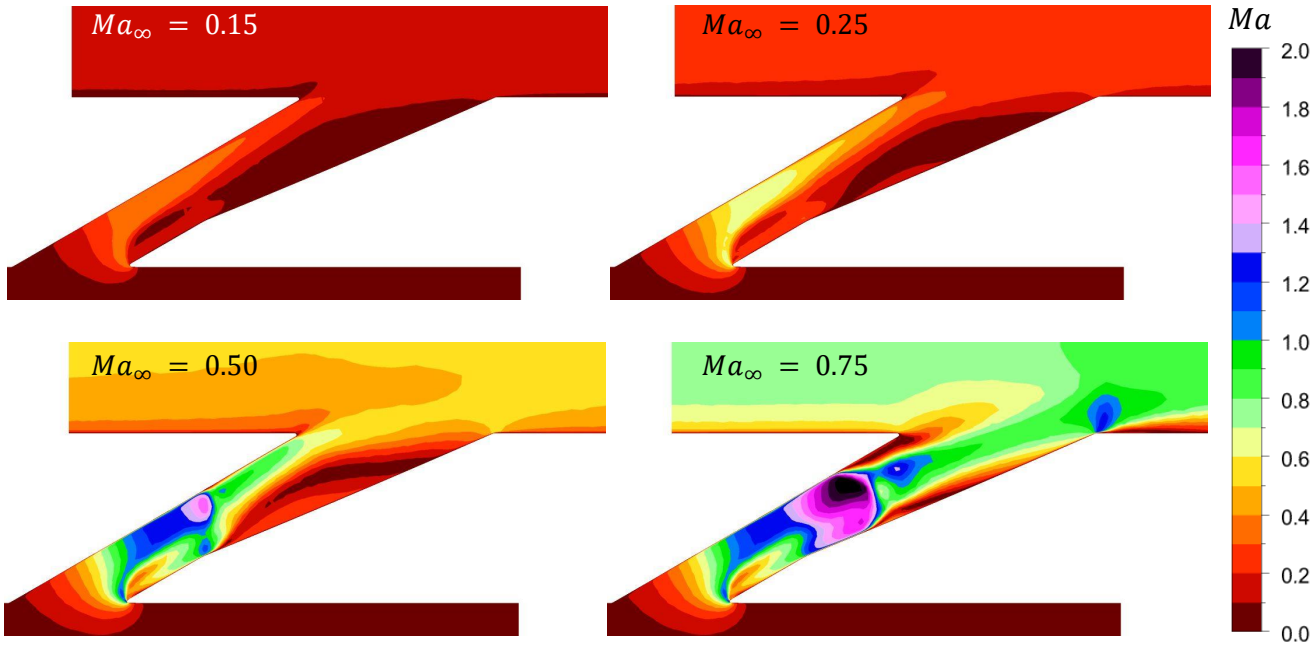

FIGURE 9: CONTOURS OF MID-PLANE MACH NUMBER FOR $\mathcal{M}$ = 1.75 AND $\mathcal{T}^\circ$=0.83

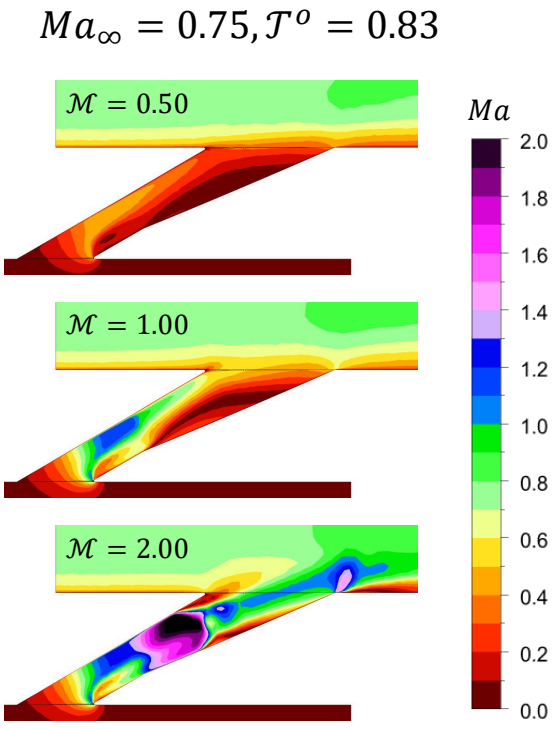

FIGURE 10: EFFECT OF $\mathcal{M}$ ON MIDPLANE *Ma* DISTRIBUTION

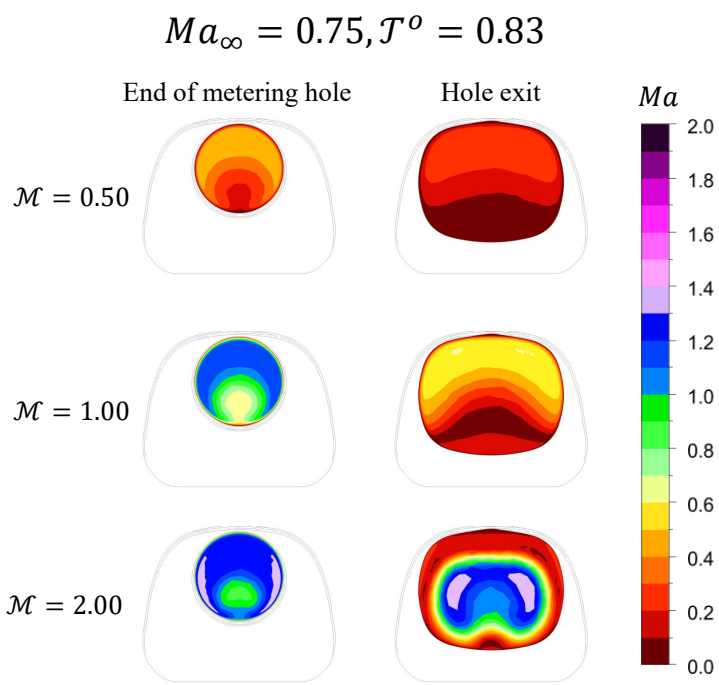

FIGURE 11: EFFECT OF $\mathcal{M}$ ON *Ma* DISTRIBUTION THROUGH THE FILM COOLING HOLE

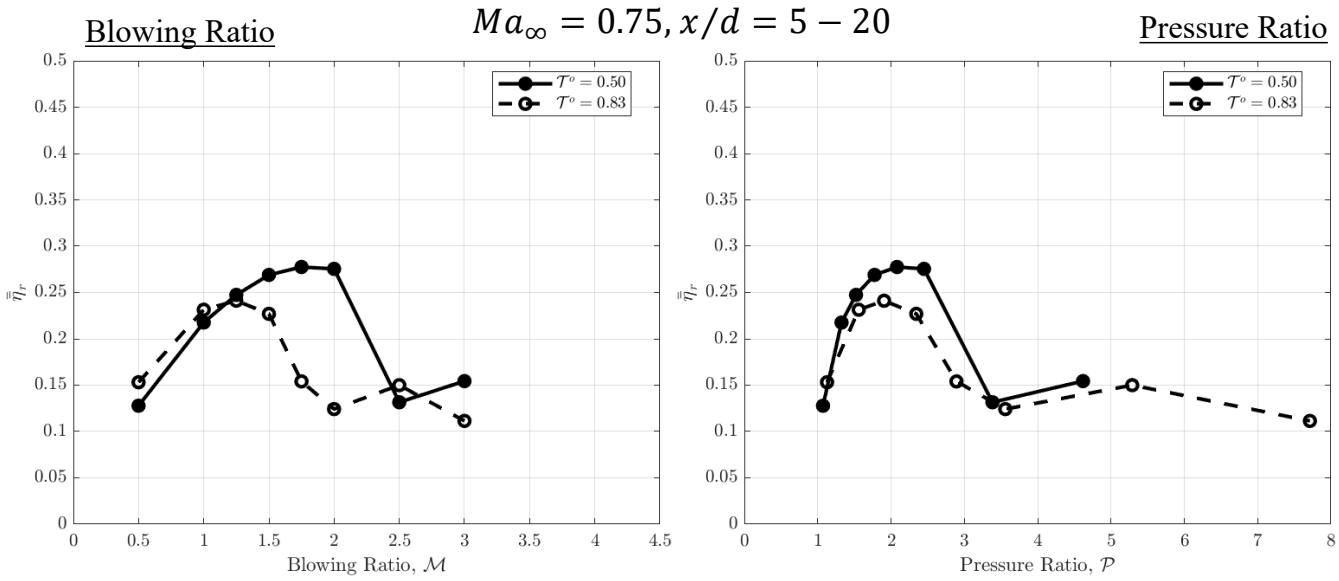

FIGURE 12: SCALING $\overline{\overline{\eta^r}}$ WITH VARYING $\mathcal{T}^\circ$

shockwaves that were observed in the previous Mach number contours. The jet separation propagates downstream, leading to a drastic decrease in effectiveness. It is also worth noting the large pressure ratios required to achieve combined high stagnation temperature ratio and high Mach number. As the stagnation temperature ratio decreases (i.e., coolant temperature decreases relative to mainstream) the static pressure ratio required for a given blowing ratio decreases, due to the requisite mass flowrate increase from the increased density of cooling gas. This in turn results in a higher peak performing blowing ratio for $\mathcal{T}^0 = 0.50$, with a drop off in performance at $\mathcal{M} > 2.0$, vs at $\mathcal{M} > 1.5$ when $\mathcal{T}^0 = 0.50$

Interestingly, there is a noticeable increase in performance at $\mathcal{P} \approx 5$. The behavior of the jet at these high pressure ratio conditions was significantly different from the other cases due to strength of the associated shock train. However, as these results are at a pressure ratio far exceeding that of a typical gas turbine cooling scheme, detailed investigation is left for future studies.

CONCLUSION

An investigation into transonic, compressible film cooling was performed with RANS simulations. These high Mach number flows are common in modern gas turbines operating near the speed of sound, but relatively little investigation has been made into the related physics involved in film cooling.

In the definition of adiabatic effectiveness, an extension from the incompressible definitions of adiabatic effectiveness is necessary to account for several inconsistencies in compressible film cooling. The viscous dissipation and kinetic energy contained in the flow mean that the wall temperature will be somewhere between a stagnation and static state, but not at either end. The recovery factor accounts for this, and the commonly used definition with mainstream recovery temperatures solves several of the problems introduced by the stagnation temperature definition. While the mixing fraction definition implied by PSP and other concentration based techniques does not account for the viscous dissipation, it tracks closely with the recovery temperature based definitions introduced here, at least within the four cases tested. Using a coolant recovery temperature reduced the apparent adiabatic effectiveness for all cases, but had a larger effect for higher mainstream Mach number. Indeed, the observed effectiveness when accounting for coolant recovery is similar to the mixing fraction definition until $Ma_\infty = 0.75$.

Observable effects of high Mach number can be seen in the midplane contours and adiabatic effectiveness averages shown. Once the flow reaches high Mach number, the coolant jet will generally shock, resulting in a separated jet and poor diffusing performance. These behaviors This poor performance also affected the flow downstream effectiveness of the hole, resulting in stark decreases in adiabatic effectiveness at high pressure ratio.

A great deal of effort is necessary to investigate the scaling and performance of film cooling at high Mach numbers. Further studies must seek to understand the effect that stagnation temperature ratio plays in the scaling of effectiveness, as well as the use of $\mathcal{P}$ for the scaling of compressibility effects. Future film cooling hole designs should mitigate the shockwave phenomena observed within this study, and to improve high Mach performance for film cooling of transonic turbine components.

ACKNOWLEDGEMENT

This paper is based upon work supported by the National Science Foundation GOALI program Award Number 1936676, and by the Department of Energy under Award Number DE-FE0025011. This report was prepared as an account of work sponsored by an agency of the United States Government. Neither the United States Government nor any agency thereof, nor any of their employees, makes any warranty, express or implied, or assumes any legal liability or responsibility for the accuracy,

completeness, or usefulness of any information, apparatus, product, or process disclosed, or represents that its use would not infringe privately owned rights. Reference herein to any specific commercial product, process, or service by trade name, trademark, manufacturer, or otherwise does not necessarily constitute or imply its endorsement, recommendation, or favoring by the United States Government or any agency thereof. The views and opinions of authors expressed herein do not necessarily state or reflect those of the United States Government or any agency thereof.

REFERENCES

[1] Liess, C. "Experimental Investigation of Film Cooling With Ejection From a Row of Holes for the Application to Gas Turbine Blades." *Journal of Engineering for Power* Vol. 97 No. 1 (1975): pp. 21–27. DOI 10.1115/1.3445904.

[2] Baldauf, Stefan and Scheurlen, Michael. "CFD Based Sensitivity Study of Flow Parameters for Engine Like Film Cooling Conditions." *Volume 4: Heat Transfer; Electric Power; Industrial and Cogeneration*: p. V004T09A037. 1996. American Society of Mechanical Engineers, Birmingham, UK. DOI 10.1115/96-GT-310.

[3] Wittig, S., Schulz, A., Gritsch, M. and Thole, K. A. "Transonic Film-Cooling Investigations: Effects of Hole Shapes and Orientations." *Volume 4: Heat Transfer; Electric Power; Industrial and Cogeneration*: p. V004T09A026. 1996. American Society of Mechanical Engineers, Birmingham, UK. DOI 10.1115/96-GT-222.

[4] Gritsch, M., Schulz, A. and Wittig, S. "Discharge Coefficient Measurements of Film-Cooling Holes With Expanded Exits." *Volume 3: Heat Transfer; Electric Power; Industrial and Cogeneration*: p. V003T09A030. 1997. American Society of Mechanical Engineers, Orlando, Florida, USA. DOI 10.1115/97-GT-165.

[5] Gritsch, M., Schulz, A. and Wittig, S. "Adiabatic Wall Effectiveness Measurements of Film-Cooling Holes With Expanded Exits." *Volume 3: Heat Transfer; Electric Power; Industrial and Cogeneration*: p. V003T09A029. 1997. American Society of Mechanical Engineers, Orlando, Florida, USA. DOI 10.1115/97-GT-164.

[6] Ligrani, P. M., Saumweber, C., Schulz, A. and Wittig, S. "Shock Wave - Film Cooling Interactions in Transonic Flows." *Volume 3: Heat Transfer; Electric Power; Industrial and Cogeneration*: p. V003T01A019. 2001. American Society of Mechanical Engineers, New Orleans, Louisiana, USA. DOI 10.1115/2001-GT-0133.

[7] Saumweber, Christian and Schulz, Achmed. "Free-Stream Effects on the Cooling Performance of Cylindrical and Fan-Shaped Cooling Holes." *Journal of Turbomachinery* Vol. 134 No. 6 (2012): p. 061007. DOI 10.1115/1.4006287.

[8] Zhou, Wenwu, Johnson, Blake and Hu, Hui. "Effects of Flow Compressibility and Density Ratio on Film Cooling Performance." *Journal of Propulsion and Power* Vol. 33 No. 4 (2017): pp. 964–974. DOI 10.2514/1.B36275.

[9] Oliver, Todd A., Bogard, David G. and Moser, Robert D. "Large eddy simulation of compressible, shaped-hole film cooling." *International Journal of Heat and Mass Transfer* Vol. 140 (2019): pp. 498–517. DOI 10.1016/j.ijheatmasstransfer.2019.04.119.

[10] Gutierrez, Daniel, Yoon, Christopher, Furgeson, Michael T., Veley, Emma M., Bogard, David G. and Thole, Karen A. "Experimental Evaluation of Adjoint Based Optimized Film Cooling Holes - Part I: Baseline Adiabatic and Overall Cooling Effectiveness." *Proceedings of ASME Turbo Expo 2022*. 2022. Rotterdam, Netherlands. DOI 10.1115/GT2022-83436.

[11] Yoon, Christopher, Gutierrez, Daniel, Furgeson, Michael T. and Bogard, David G. "Evaluation of Adjoint Optimized Hole - Part II: Parameter Effects on Performance." *Volume 6A: Heat Transfer — Combustors; Film Cooling*: p. V06AT12A031. 2022. American Society of Mechanical Engineers, Rotterdam, Netherlands. DOI 10.1115/GT2022-82726.

[12] Anderson, Joshua B., Boyd, Emily J. and Bogard, David G. "Experimental Investigation of Coolant-to-Mainstream Scaling Parameters With Cylindrical and Shaped Film Cooling Holes." *Volume 5B: Heat Transfer*: p. V05BT12A033. 2015. American Society of Mechanical Engineers, Montreal, Canada. DOI 10.1115/GT2015-43072.

[13] Shih, T.-H., Liou, W. W., Shabbir, A., Yang, Z. and Zhu, J. "A New K-epsilon Eddy Viscosity Model for High Reynolds Number Turbulent Flows: Model Development and Validation." *Technical Memorandum 10672*. 1994. National Aeronautics and Space Administration.

[14] *Fluent Theory Guide 12.0*. ANSYS, Inc. (2009).

[15] Richardson, Lewis Fry and Gaunt, J. Aurthur. "VIII. The deferred approach to the limit." *Philosophical Transactions of the Royal Society of London. Series A, Containing Papers of a Mathematical or Physical Character* Vol. 226 No. 636-646 (1927): pp. 299–361. DOI 10.1098/rsta.1927.0008.

[16] Van Driest, E. R. "Turbulent Boundary Layer in Compressible Fluids." *Journal of the Aeronautical Sciences* Vol. 18 No. 3 (1951): pp. 145–160. DOI 10.2514/8.1895.

[17] Furukawa, Tetsuji and Ligrani, Phillip M. "Transonic Film Cooling Effectiveness from Shaped Holes on a Simulated Turbine Airfoil." *Journal of Thermophysics and Heat Transfer* Vol. 16 No. 2 (2002): pp. 228–237. DOI 10.2514/2.6672.

[18] Nasir, Shakeel, Bolchoz, Trey, Ng, Wing-Fai, Zhang, Luzeng J., Koo Moon, Hee and Anthony, Richard J. "Showerhead Film Cooling Performance of a Turbine Vane at High Freestream Turbulence in a Transonic Cascade." *Journal of Turbomachinery* Vol. 134 No. 5 (2012): p. 051021. DOI 10.1115/1.4004200.

[19] Xue, Song, Ng, Wingfai, Ekkad, S., Moon, H. K. and Zhang, Luzeng. "The Performance of fan-shaped hole film cooling on a gas turbine blade at transonic conditon with high freestream turbulence." *50th AIAA Aerospace Sciences Meeting including the New Horizons Forum and Aerospace Exposition*. 2012. American Institute of Aeronautics and Astronautics. DOI 10.2514/6.2012-368.

[20] Ornano, Francesco and Povey, Thomas. "Theory of Non-Dimensional Groups in Film Effectiveness Studies." *Journal of Turbomachinery* Vol. 142 No. 4 (2020): p. 041002. DOI 10.1115/1.4046277.